Ecofriendly Cellulose Substrate-Based Flexible Transparent Electrode for Flexible Organic Solar Cells with Efficiency Over 18%

Zheng Xiao, Shitong Li, Jian Liu, Xin Chen, Zhaochen Suo, Chenxi Li, Xiangjian Wan,* and Yongsheng Chen*

Flexibility is a key advantage of organic solar cells (OSCs), and the power conversion efficiencies (PCEs) of flexible OSCs (FOSCs) are primarily constrained by flexible transparent electrodes (FTEs). While much attention has been devoted to the study of conductive layers on FTEs, the importance of flexible substrates in influencing the properties of FTEs and the performance of FOSCs is often overlooked. In this study, an FTE is developed using an eco-friendly ethyl cellulose (EC) substrate and silver nanowires (AgNWs) as the conductive electrode. The FTE exhibits a high transmittance of up to 88% at 550 nm and a low sheet resistance of 17.65 Ω/□. Consequently, FOSCs based on the EC/PI FTEs achieve a remarkable PCE of 18.05%, comparable to that on the rigid ITO substrate. The flexible devices also demonstrate excellent bending and peeling durability even under extreme bending conditions.

1. Introduction

As one of the promising green energy technologies, organic solar cells (OSCs) have shown great potential for various applications, e.g., building-integrated photovoltaic systems and wearable electronics.[1] In contrast to inorganic photovoltaic devices, which are hampered by the intrinsic brittle nature of inorganic semiconductor materials, OSCs offer the advantage of intrinsic flexibility due to the properties of organic semiconductor materials.[2] Significant progress has recently been achieved in OSCs, with remarkable efficiencies exceeding 19% reported in devices on rigid substrates.[3] However, the performance of flexible organic solar cells (FOSCs) have significantly lagged behind that of rigid substrate-based devices primarily due to the absence of ideal flexible transparent electrodes (FTEs).[4] The most commonly used flexible electrode is indium tin oxide (ITO) sputtered on a polyethylene terephthalate (PET) substrate.[5] However, the PET/ITO

electrode suffers from the brittleness of ITO and the cost and scarcity issues associated with indium.[6] Consequently, various FTEs, such as PEDOT:PSS, carbon nanotubes, graphene, and silver nanowires (AgNWs), have been studied for FOSCs.[7] Among them, AgNW-based FTEs have demonstrated great potential with high conductivity, transparency, and ease of solution processing.[8] It is worth noting that more attention has been focused on the conducting layer for FTEs. However, few reports have focused on the study on flexible substrates. In fact, as a crucial component of FTEs, flexible substrates significantly influence the overall properties such as transparency, thermal resistance, and mechanical properties of FTEs.[9] There are some specific requirements for flexible substrates. First, a smooth surface and nonporous structure are required to avoid the discontinuities of conducting films on them.[10] Second, the substrate should withstand high temperatures without deformations depending on the applications.[11] Additionally, considerations of cost and process ease should also be taken into account.[12]

Polymers stand out as the optimal candidates for flexible substrates in FOSCs. PET and polyimide (PI) are widely used as flexible substrates for FTEs.[13] However, the limited thermal tolerance of PET, attributed to a low glass transition temperature (T_g) and a high coefficient of thermal expansion (70–80 ppm K^{-1}), hinders its application in FOSCs, despite widespread use on the laboratory scale.[14] PI, another commonly used polymer substrate in FOSCs, boasts outstanding mechanical properties and an exceptionally high $T_g > 200\,°C$.[15] Nevertheless, only super thin (<10 μm) PI shows decent transmittance, and freestanding PI films generally exhibits relatively low transmittance, leading to reduced currents and low PCEs in corresponding FOSCs.[16] Consequently, there is a need to develop flexible substrates that simultaneously offer high transmittance, excellent thermal resistance, and superior mechanical properties.

Cellulose is an abundant and eco-friendly polymer.[17] It has the high T_g and low CTE (2-5 ppm K^{-1}) and is a good alternative as flexible substrate for FTEs.[18] Cellulose, particularly films based on cellulose nanocrystals (CNCs) and cellulose nanofibers (CNFs), has been extensively explored as flexible substrates in

Z. Xiao, S. Li, J. Liu, X. Chen, Z. Suo, C. Li, X. Wan, Y. Chen
State Key Laboratory of Elemento-Organic Chemistry
Key Laboratory of Functional Polymer Materials, College of Chemistry
Renewable Energy Conversion and Storage Center (RECAST)
Nankai University
Tianjin 300071, China
E-mail: xjwan@nankai.edu.cn; yschen99@nankai.edu.cn

organic electronics, including OSCs.[10d,19] For example, Zhou et al. reported polymer solar cells based on CNC substrate and a thin-layer Ag as FTEs and achieved a power conversion efficiency of 2.7%.[20] Lin et al. used CNFs as flexible substrates and developed an FTE by embedding silver nanowires (Ag NWs) into CNFs. F-OSC using the FTE and PM6:Y6 as active layer delivered a PCE of 7.47%.[14c] The relatively low efficiency was mainly caused by the large surface roughness and low transmittance, posing a bottleneck that restricts the application of CNCs and CNFs as flexible substrates in FOSCs.[21] As a low-cost chemically modified cellulose derivative, ethyl cellulose (EC) exhibits unique properties, including high transparency, favorable flexibility, and good thermal stability. These characteristics make it an excellent alternative as a flexible substrate for preparing flexible electrodes.

In this study, we prepared an FTE using an EC substrate and AgNWs. To address the surface roughness caused by the crystallinity of EC and enhance mechanical properties, a 0.7 μm thin layer of PI was coated onto the EC film. Remarkably, this optimized EC/PI substrate maintained a transmittance exceeding 90% across the 300–1000 nm range, with minimal impact on transparency. The resulting FTE, built on this flexible substrate, achieves a high transmittance of up to 88% at 550 nm and a low sheet resistance of 17.65 Ω/□. Utilizing this FTE, FOSCs with PM6:L8-BO as the active layer were fabricated, showing a remarkable PCE of 18.05%, comparable to that achieved on rigid ITO substrates. Moreover, the FOSCs exhibited excellent mechanical properties, retaining 95% efficiency after 5000 bends at a radius of 1 mm.

2. Results and Discussion

As depicted in **Figure 1**a, PI and EC are sequentially deposited on the glass substrate. Subsequently, the flexible hybrid film EC/PI

is carefully peeled off, exhibiting a minimal roughness of approximately 0.8 nm (as shown in Figure S1, Supporting Information). AgNWs are then deposited on the hybrid substrate to form an FTE using the method previously reported by our group. For the production of a free-standing film with high transmittance, the thicknesses of EC and PI are optimized at 90 and 0.7 μm, respectively. The transmittance spectra of EC and EC/PI, along with a 40 μm thick PI film for comparison, are illustrated in Figure 1b.

The free-standing EC film with a thickness of 90 μm shows a high transmittance over 90% in the range 300–1000 nm. Evidently, a thin 0.7 μm PI layer only slightly reduces the transmittance of the EC film in the range of 300–1000 nm. It primarily acts as a shield against ultraviolet light below 300 nm, which is advantageous considering that most organic semiconductor materials exhibit no absorptions below this wavelength. Moreover, UV shielding can enhance the stability of the device.[15a] For comparison, the transmittance of the free-standing 40 μm thick PI film is considerably lower than that of EC and EC/PI. At 550 nm, the PI film shows a transmittance of 85.91%, much lower than that the EC/PI film with the value of 91.39%. It is worth noting that the hybrid EC/PI film can be easily prepared on a large area using the doctor-blading method, as depicted in Figure 1c. As illustrated in Figure S2a (Supporting Information), the EC/PI film exhibits higher stretchability than the EC film due to the lower Young's modulus of PI compared with EC.[22] To elucidate the mechanism behind the enhanced mechanical property, cross-section SEM images of EC/PI and EC were examined. As shown in Figure 1d, EC and PI are closely bound together, with some pores and defects inside the EC film (as shown in Figure S2b, Supporting Information) attributed to air bubbles in the EC solution and the crystallinity of EC (Figure S3, Supporting Information) during the film formation process. The water vapor transmission rate (WVTR) and
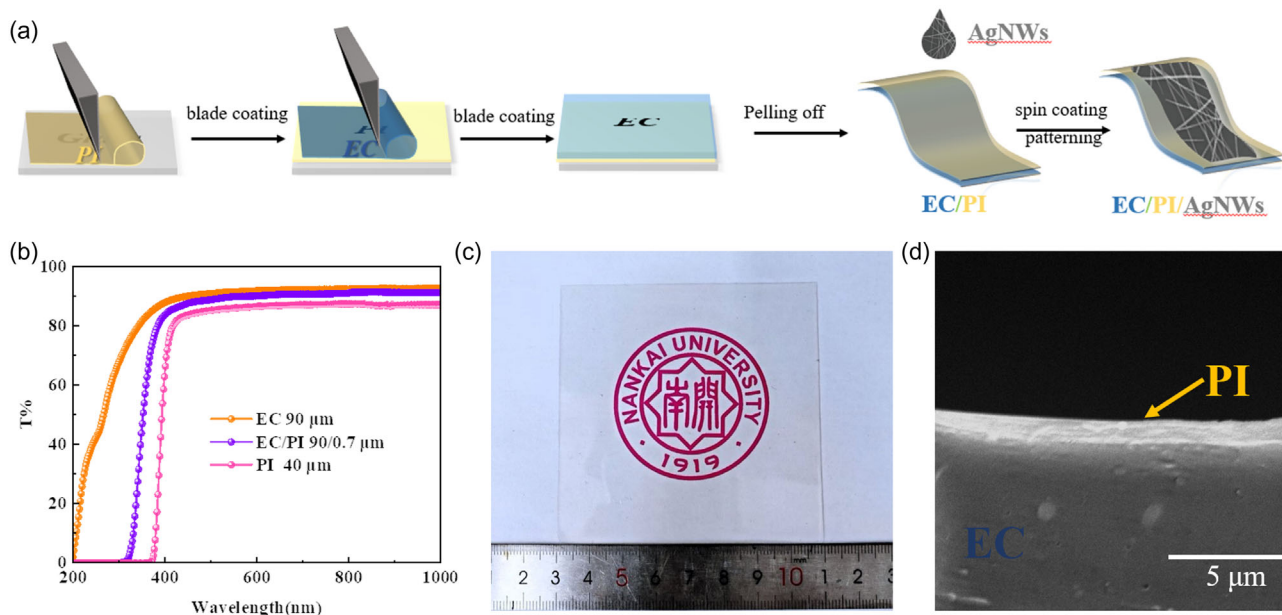

Figure 1. a) Schematic of the fabrication of EC/PI/AgNWs. b) Transmittance spectra of the EC, EC/PI, and PI film. c) Photograph of the flexible substrate in the scale of 8 cm × 8 cm. d) Cross-section SEM image of the flexible substrate.

oxygen transmission rate (OTR) of the EC film were measured, yielding values of 210 g/[m²-day] and 19 cc/[m²-day], respectively, which are higher than those of conventional PET and PI (as shown in Table S1, Supporting Information). This is primarily due to the presence of unsubstituted –OH groups in EC (around 48.0–49.5%) and defects within the EC film. Following the deposition of a 0.7 µm PI layer, the WVTR and OTR of EC/PI film decreased to 120 g/[m²-day] and 11 cc/[m²-day], respectively.

Utilizing the aforementioned hybrid flexible substrate, an FTE was prepared by coating a layer of AgNWs using the method previously reported by our group.[23] Figure S4 (Supporting Information) illustrates a homogeneous distribution of AgNWs formed on the hybrid flexible substrate. As shown in **Figure 2**a, the FTE exhibits an average transmittance of over 88.24% in the wavelength range of 500–1000 nm and the highest transmittance of 88.05% at 550 nm, and a low sheet resistance of 17.65 $\Omega/\square$. In comparison, the commercial PET/ITO exhibits clearly lower transparency than the above FTE, especially in the near-infrared range.

Figure 2b depicts the normalized sheet resistance during bending cycles for PET/ITO and PI/EC/AgNW-based FTEs. After 1000 bending cycles with a radius of 5 mm, the resistance of PET/ITO and PI/EC/AgNWs remains essentially unchanged. However, when the bending radius is reduced to 3 mm, the resistance of PET/ITO increases 14.51 times after 1000 bends, and further reducing the bending radius to 1 mm results in a resistance increase of 98.20 times. In contrast, the resistance of EC/PI/AgNWs remains consistent, even with a curvature radius reduced to 1 mm. To further demonstrate the outstanding mechanical robustness of EC/PI/AgNWs, the FTE underwent up to 10 000 bending cycles with a bending radius of 1 mm. As depicted in Figure 2c, the resistance of EC/PI/AgNWs increased only 1.16 times the initial resistance after 10 000 bending cycles. Alongside the aforementioned photoelectric parameters, these excellent mechanical properties position EC/PI/AgNWs as a highly suitable material for FOSCs.

With the combined high-performance features of EC/PI/AgNWs, FOSCs with PM6 and L8-BO as active layers are fabricated. The detailed fabrication procedure can be found in the SI. The current density versus voltage (J–V) curves of the flexible

devices and the corresponding devices based on rigid ITO on glass and flexible ITO on PET were characterized and compared, as presented in **Figure 3**b. The photovoltaic parameters of these devices are summarized in **Table 1**. The OSC based on glass-ITO exhibited an open-circuit voltage (V_{oc}) of 0.876 V, short-circuit current density (J_{sc}) of 26.22 mA cm^{-2}, fill factor (FF) of 80.00%, and PCE of 18.36%. Due to the excellent properties of EC/PI/AgNWs, the FOSCs based on EC/PI/AgNWs achieved a PCE of 18.05%, with a V_{oc} of 0.875 V, a J_{sc} of 26.38 mA cm^{-2}, and an FF of 78.26%, representing one of the best reported PCEs for a single-junction flexible OSC (as shown in Table S2, Supporting Information), comparable to that of the rigid OSC based on glass-ITO. In contrast, flexible devices based on PET/ITO exhibited a PCE of 15.58%, with a V_{oc} of 0.865 V, a relatively low J_{sc} of 22.85 mA cm^{-2}, an FF of 78.83%.

The J_{sc} values of the aforementioned devices with different electrodes were confirmed by the corresponding external quantum efficiency (EQE) measurements, as shown in Figure 3c. The EQE spectrum of the EC/PI/AgNWs-based FOSCs exhibited higher values in the wavelength range from 650 to 850 nm compared to the glass/ITO-based reference device. These results can be attributed to the high transmittance of EC/PI/AgNWs, thus enhancing the light absorption of the active layer.

With the excellent performance of these EC/PI/AgNWs-based FOSCs, the flexibility and mechanical robustness of FOSCs were further investigated under various bending conditions. In **Figure 4**a, the normalized efficiency of FOSCs after 1000 bending cycles with various curvature radii is presented. The efficiency of PET/ITO-based FOSCs decreased significantly when the radius of curvature was reduced from 5 mm to 1 mm. The PCE is almost zero due to the sharp rise in resistance of the PET/ITO. In contrast, EC/PI/AgNW-based FOSCs exhibit outstanding flexibility and mechanical robustness, maintaining the initial PCE even with a bending radius of 1 mm. Therefore, EC/PI/AgNW-based FOSCs were further tested for up to 5000 cycles at a fixed bending radius of 1 mm. As demonstrated in Figure 4b, after 5000 consecutive bending cycles, the PCE only drops by about 4.42% of the initial value. To our knowledge, this is the best mechanical performance of FOSCs to date, with a PCE of more than 18%. Figure 4c shows the influence of 5000 bending cycles of 1 mm on FOSCs' photovoltaic
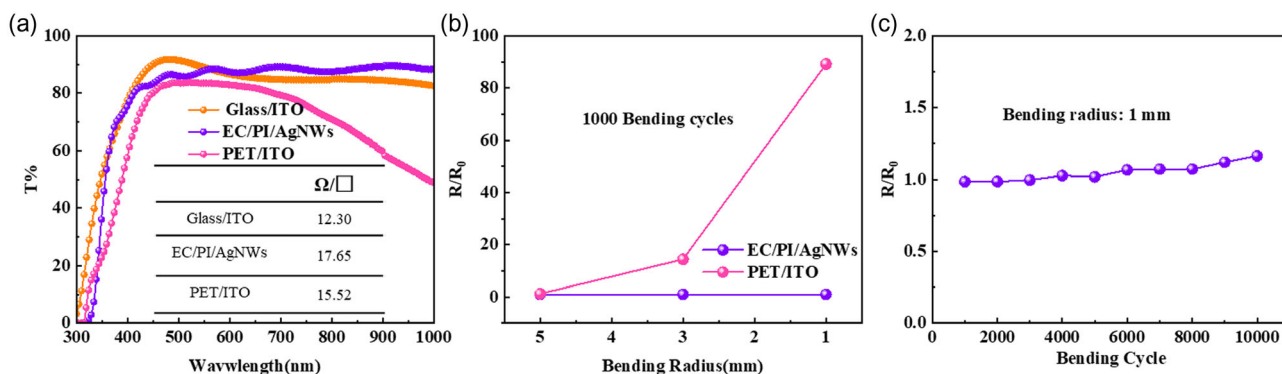

Figure 2. a) Transmittance spectra of the glass/ITO, EC/PI/AgNWs electrode and PET/ITO films. b) The normalized square resistance of the EC/PI/AgNWs electrode and PET/ITO after 1000 bending tests with different radii. c) The normalized square resistances of the EC/PI/AgNWs electrode during 10 000 bending cycles at a fixed bending radius of 1 mm.
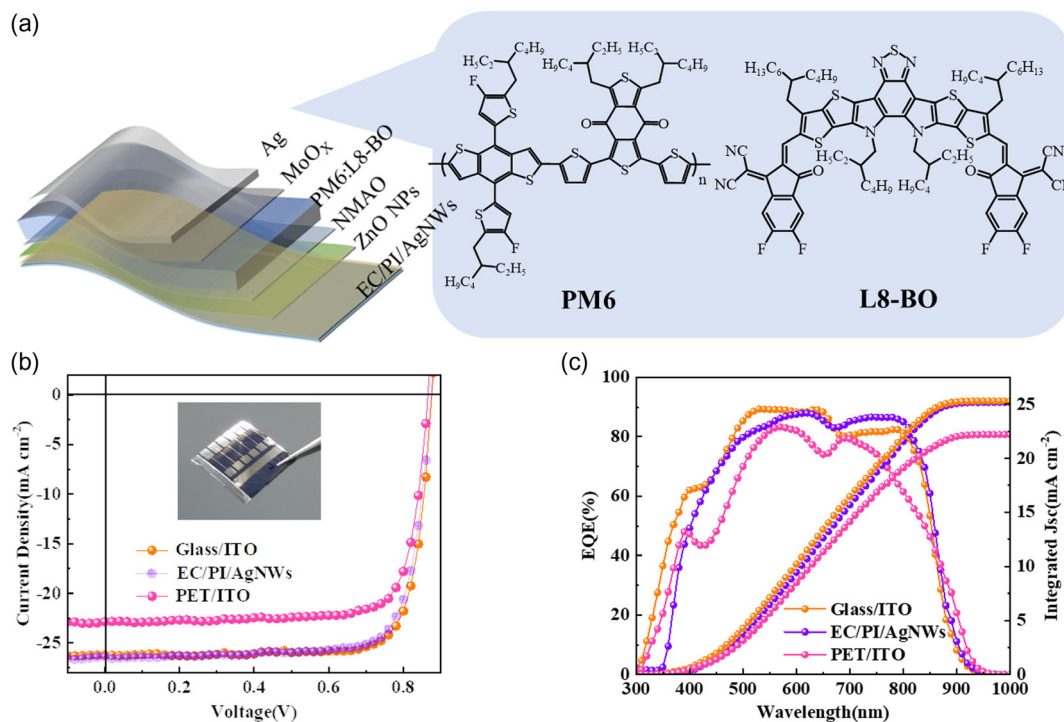
Figure 3. a) Structure of the FOSC based on the EC/PI/AgNWs electrode, including chemical structures of PM6 and L8-BO. b) J–V curves and c) EQE spectra and the integrated J_{sc} of a typical device (PM6:L8-BO) based on glass ITO, EC/PI/AgNWs, and PET/ITO.

Table 1. Photovoltaic parameters of the OSCs devices based on glass ITO, EC/PI/AgNWs and PET/ITO with PM6 and L8-BO.

Electrode	V_{oc} [V]	J_{sc} [mA cm^{-2}]	FF [%]	PCE$_{max}$ (PCE$_{ave}$)[a] [%]
Glass/ITO	0.876	26.22	80.00	18.36 (18.17 ± 0.14)
EC/PI/AgNWs	0.875	26.38	78.26	18.05 (17.83 ± 0.16)
PET/ITO	0.865	22.85	78.83	15.58 (15.20 ± 0.24)

[a]The average PCE values were calculated from 10 devices.

performance parameters, where the decline in PCE is mainly caused by a drop in J_{sc} (about 4.38%), while the changes in V_{oc} (decreased by about 0.1%) and the FF (increased by about 0.1%) are negligible. The slightly reduced J_{sc} might be due to the increased resistance and charge carrier recombination for FOSCs after bending. In addition, we conducted an initial stability study of the EC/PI/AgNW-based FOSC. As depicted in Figure S5 (Supporting Information), the flexible device exhibited outstanding shelf stability, with efficiency remaining at 93.85% after 450 h of storage in a glove box filled with N$_2$. Furthermore, as shown in Figure S6 (Supporting Information),
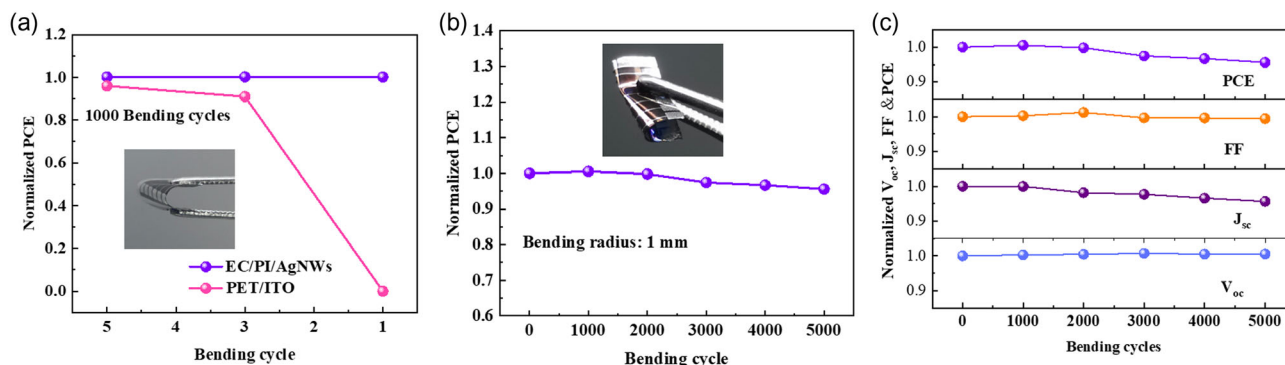

Figure 4. a) The normalized PCE of the FOSCs based on EC/PI/AgNWs and PET/ITO after 1000 bending cycles at various bending radius. b) The normalized PCE and c) the normalized V_{oc}, J_{sc}, FF of the FOSCs based on EC/PI/AgNWs after different bending cycles at a curvature radius of 1 mm.

the device demonstrated good photostability, retaining 85.4% of its initial efficiency after 140 h of continuous illumination at the maximum power point under $100\,mW\,cm^{-2}$ LED arrays at 25 °C in an N_2 atmosphere.

3. Conclusion

In summary, we have developed a flexible substrate based on an ecofriendly material EC and prepared a transparent electrode based on the flexible substrate and AgNWs. Utilizing this flexible electrode, we successfully fabricated FOSCs that exhibited comparable performance to their rigid counterparts. Notably, our single-junction FOSCs achieved an impressive PCE of 18.05%, representing one of the highest PCE values reported for FOSCs to date. Furthermore, the FOSC demonstrated exceptional mechanical stability even under extreme bending conditions. We firmly believe that this straightforward and cost-effective approach for fabricating flexible transparent electrodes holds great promise for future applications in flexible electronics.

Supporting Information

Supporting Information is available from the Wiley Online Library or from the author.

Conflict of Interest

The authors declare no conflict of interest.

Data Availability Statement

The data that support the findings of this study are available in the supplementary material of this article.

Keywords

cellulose, flexible transparent electrode, organic solar cells

[1] a) Y. N. Sun, M. J. Chang, L. X. Meng, X. J. Wan, H. H. Gao, Y. M. Zhang, K. Zhao, Z. H. Sun, C. X. Li, S. R. Liu, H. K. Wang, J. J. Liang, Y. S. Chen, *Nat. Electron.* **2019**, *2*, 513; b) T. Y. Qu, L. J. Zuo, J. D. Chen, X. Shi, T. Zhang, L. Li, K. C. Shen, H. Ren, S. Wang, F. M. Xie, Y. Q. Li, A. K. Y. Jen, J. X. Tang, *Adv. Opt. Mater.* **2020**, *8*, 2000669; c) S. Li, Z. Li, X. Wan, Y. Chen, *eScience* **2023**, *3*, 100085; d) H. Li, Q. Chen, G. Zhang, Z. Zhang, J. Fang, C. Zhao, W. Li, *J. Mater. Chem. A* **2023**, *11*, 158.

[2] a) D. Lv, Q. Jiang, Y. Shang, D. Liu, *npj Flex. Electron.* **2022**, *6*, 38; b) S. A. Hashemi, S. Ramakrishna, A. G. Aberle, *Energy Environ. Sci.* **2020**, *13*, 685; c) J. Miao, Y. Wang, J. Liu, L. Wang, *Chem. Soc. Rev.* **2022**, *51*, 153; d) J. Qin, L. Lan, S. Chen, F. Huang, H. Shi, W. Chen, H. Xia, C. Sun, C. Yang, *Adv. Funct. Mater.* **2020**, *30*, 2002529.

[3] a) J. Fu, P. W. K. Fong, H. Liu, C. S. Huang, X. Lu, S. Lu, M. Abdelsamie, T. Kodalle, C. M. Sutter-Fella, Y. Yang, G. Li, *Nat. Commun.* **2023**, *14*, 1760; b) Z. Chen, H. Yao, J. Wang, J. Zhang, T. Zhang, Z. Li, J. Qiao, S. Xiu, X. Hao, J. Hou, *Energy Environ. Sci.* **2023**, *16*, 2637; c) X. Zheng, X. Wu, Q. Wu, Y. Han, G. Ding, Y. Wang, Y. Kong, T. Chen, M. Wang, Y. Zhang, J. Xue, W. Fu, Q. Luo, C. Ma, W. Ma, L. Zuo, M. Shi, H. Chen, *Adv. Mater.* **2023**, *36*, 2307280.

[4] a) Z. Chen, J. Zhu, D. Yang, W. Song, J. Shi, J. Ge, Y. Guo, X. Tong, F. Chen, Z. Ge, *Energy Environ. Sci.* **2023**, *16*, 3119; b) M. R. Azani, A. Hassanpour, T. Torres, *Adv. Energy Mater.* **2020**, *10*, 2002536; c) J. Wang, K. Fukuda, D. Inoue, D. Hashizume, L. Sun, S. Xiong, T. Yokota, T. Someya, *ACS Appl. Mater. Interfaces* **2022**, *14*, 14165; d) C. Jia, X. Zhao, Y.-H. Lai, J. Zhao, P.-C. Wang, D.-S. Liou, P. Wang, Z. Liu, W. Zhang, W. Chen, Y.-H. Chu, J. Li, *Nano Energy* **2019**, *60*, 476.

[5] J. Wang, L. Sun, S. Xiong, B. Du, T. Yokota, K. Fukuda, T. Someya, *ACS Appl. Mater. Interfaces* **2023**, *15*, 21314.

[6] a) A. De Sio, K. Chakanga, O. Sergeev, K. von Maydell, J. Parisi, E. von Hauff, *Sol. Energy Mater. Sol. Cells* **2012**, *98*, 52; b) T. Dinh-Phuc, L. Hung-I, L. Chih-Kuang, *Coatings* **2018**, *8*, 212.

[7] a) D. Zhang, A. H. Alami, W. C. H. Choy, *Sol. RRL* **2021**, *6*, https://doi.org/10.1002/solr.202100830; b) X. Zheng, L. Zuo, K. Yan, S. Shan, T. Chen, G. Ding, B. Xu, X. Yang, J. Hou, M. Shi, *Energy Environ. Sci.* **2023**, *16*, 2284; c) W. Zha, L.-M. Chen, S. Sun, X. Gao, Y. Han, T. Liu, Q. Luo, Y.-C. Chao, H.-W. Zan, H.-F. Meng, X. Zhu, C.-Q. Ma, *Sol. RRL* **2023**, *7*, 2300322; d) Y. F. Zhang, H. Ren, J. D. Chen, H. Y. Hou, H. M. Liu, S. Tian, W. S. Chen, H. R. Ge, Y. Q. Li, H. Mao, Z. Su, J. X. Tang, *Adv. Funct. Mater.* **2023**, *33*, 2212260; e) J. X. Song, G. Q. Ma, F. Qin, L. Hu, B. W. Luo, T. F. Liu, X. X. Yin, Z. Su, Z. B. Zeng, Y. Y. Jiang, G. N. Wang, Z. F. Li, *Polymers* **2020**, *12*, 450; f) J. Wan, X. Fan, Y. Li, P. Li, T. Zhang, K. N. Hui, H. Huang, K. Kang, L. Qian, *Front. Chem.* **2021**, *9*, 807538.

[8] a) G. Zeng, W. Chen, X. Chen, Y. Hu, Y. Chen, B. Zhang, H. Chen, W. Sun, Y. Shen, Y. Li, F. Yan, Y. Li, *J. Am. Chem. Soc.* **2022**, *144*, 8658; b) H. Y. Hou, Y. F. Zhang, J. D. Chen, *Chem. Eng. J.* **2022**, *263*, 118084.

[9] D. D. Li, W. Y. Lai, Y. Z. Zhang, W. Huang, *Adv. Mater.* **2018**, *30*, 1704738.

[10] a) Y. U. Kim, S. H. Park, N. T. Nhan, M. H. Hoang, M. J. Cho, D. H. Choi, *Macromol. Res.* **2021**, *29*, 75; b) S. Lee, E. H. Kim, S. Yu, H. Kim, C. Park, S. W. Lee, H. Han, W. Jin, K. Lee, C. E. Lee, J. Jang, C. M. Koo, C. Park, *ACS Nano* **2021**, *15*, 8940; c) H. C. Kwon, W. Jeong, Y. S. Lee, J. H. Jang, H. S. Jeong, S. Kim, D. Song, A. Park, E. Noh, K. Lee, H. Kang, *Adv. Energy Mater.* **2022**, *13*, 2200023; d) S. Dai, Y. Chu, D. Liu, F. Cao, X. Wu, J. Zhou, B. Zhou, Y. Chen, J. Huang, *Nat. Commun.* **2018**, *9*, 2737.

[11] a) J. Jang, J. H. Kim, S. Lee, C. M. Oh, I. W. Hwang, S. Kim, A. Park, D. Kang, C. Jang, T. Ki, H. Kim, K. Lee, *ACS Appl. Energy Mater.* **2023**, *6*, 9778; b) H. N. Tran, C. B. Park, J. H. Lee, J. H. Seo, J. Y. Kim, S. H. Oh, S. N. Cho, *Small* **2023**, https://doi.org/10.1002/smll.202307441.

[12] Y. P. Xie, H. Lu, J. Huang, H. B. Xie, *Adv. Funct. Mater.* **2023**, *33*, 2213910.

[13] a) C. Xie, C. Xiao, J. Fang, C. Zhao, W. Li, *Nano Energy* **2023**, *107*, 108153; b) J. Wan, Y. Xia, J. Fang, Z. Zhang, B. Xu, J. Wang, L. Ai, W. Song, K. N. Hui, X. Fan, Y. Li, *Nanomicro Lett.* **2021**, *13*, 44.

[14] a) G. Zhang, Q. Chen, C. Xie, Y. Wang, C. Zhao, C. Xiao, Y. Wei, W. Li, *npj Flex. Electron.* **2022**, *6*, 37; b) N. Y. Kwon, S. H. Park, Y. Lee, G. D. Kong, H. D. Chau, H. J. Yoon, H. Y. Woo, M. H. Hoang, M. J. Cho, D. H. Choi, *ACS Appl. Mater. Interfaces* **2022**, *14*, 34909; c) P.-C. Lin, C.-T. Hsieh, X. Liu, F.-C. Chang, W.-C. Chen, J. Yu, C.-C. Chueh, *Chem. Eng. J.* **2021**, *405*, 126996.

[15] a) Y. Wang, Q. Chen, Y. Wang, G. Zhang, Z. Zhang, J. Fang, C. Zhao, W. Li, *Macromol. Rapid Commun.* **2022**, *43*, 2200432; b) X. L. Yin, J. Wang, A. L. Liu, W. Z. Cai, L. Ying, X. He, Z. F. Tang, L. T. Hou, *Flex. Print. Electron.* **2020**, *5*, 014003; c) L. Sun, W. Zeng, C. Xie, L. Hu, X. Dong, F. Qin, W. Wang, T. Liu, X. Jiang, Y. Jiang, Y. Zhou, *Adv. Mater.* **2020**, *32*, 1907840.

[16] a) X. Dong, P. Shi, L. Sun, J. Li, F. Qin, S. Xiong, T. Liu, X. Jiang, Y. Zhou, *J. Mater. Chem. A* **2019**, *7*, 1989; b) H. Kimura, K. Fukuda, H. Jinno, S. Park, M. Saito, I. Osaka, K. Takimiya, S. Umezu, T. Someya, *Adv. Mater.* **2019**, *31*, 1808033.

[17] H. Tu, M. Zhu, B. Duan, L. Zhang, *Adv. Mater.* **2020**, *33*, 2000682.

[18] a) H. Zhu, Z. Fang, C. Preston, Y. Li, L. Hu, *Energy Environ. Sci.* **2013**, *7*, 269; b) R. J. Moon, A. Martini, J. Nairn, J. Simonsen, J. Youngblood, *Chem. Soc. Rev.* **2011**, *40*, 3941.

[19] K. Oksman, Y. Aitomäki, A. P. Mathew, G. Siqueira, Q. Zhou, S. Butylina, S. Tanpichai, X. Zhou, S. Hooshmand, *Composites, Part A* **2016**, *83*, 2.

[20] Y. Zhou, C. Fuentes-Hernandez, T. M. Khan, J.-C. Liu, J. Hsu, J. W. Shim, A. Dindar, J. P. Youngblood, R. J. Moon, B. Kippelen, *Sci. Rep.* **2013**, *3*, 1536.

[21] K. Y. Lee, Y. Aitomäki, L. A. Berglund, K. Oksman, A. Bismarck, *Compos. Sci. Technol.* **2014**, *105*, 15.

[22] a) J. Huang, Z. Ren, Y. Zhang, K. Liu, H. Zhang, H. Tang, C. Yan, Z. Zheng, G. Li, *Adv. Funct. Mater.* **2021**, *31*, 2010172; b) S. De, J. N. Coleman, *MRS Bull.* **2011**, *36*, 774.

[23] Y. Sun, L. Meng, X. Wan, Z. Guo, X. Ke, Z. Sun, K. Zhao, H. Zhang, C. Li, Y. Chen, *Adv. Funct. Mater.* **2021**, *31*, 2010000.